DOI: 10.1002/chem.200903384

Complex–Surfactant-Assisted Hydrothermal Synthesis and Properties of Hierarchical Worm-Like Cobalt Sulfide Microtubes Assembled by Hexagonal Nanoplates

Bo Liu,[a] Shuang Wei,[b] Yan Xing,*[a] Dan Liu,[c] Zhan Shi,[c] Xianchun Liu,[a] Xiujuan Sun,[a] Suying Hou,[a] and Zhongmin Su*[a]

Abstract: The preparation of exquisite hierarchical worm-like $Co_{1-x}S$ ($x = 0.75$) microtubes by a one-pot complex–surfactant-assisted hydrothermal method is successfully achieved for the first time. The hierarchical structures of the microtube wall are assembled from numerous interleaving hexagonal nanoplates. X-ray diffraction, X-ray photoelectron spectroscopy, scanning electron microscopy, transmission electron microscopy, and high-resolution transmission electron microscopy were used to characterize the samples. The experimental results indicate that the "soft template" surfactant cetyltrimethylammonium bromide and the chelating ethylenediamine both play important roles for the formation of hierarchical $Co_{1-x}S$ microtubes. A possible formation mechanism for the growth processes is proposed. Additionally, the electrochemical and magnetic properties of $Co_{1-x}S$ microtubes were systematically studied.

Keywords: cobalt · electrochemistry · magnetic properties · microtubes · surfactants

Introduction

Recently, synthesis of hierarchical structures based on the assembly of nanoscale building blocks has attracted significant interest from chemists and materials scientists owing to their novel functions in the development of advanced devices and systems.[1] Hierarchical micro- and nanostructures with hollow interiors are of particular interest because of their potential for wide-ranging applications, especially in optical, electronic, magnetic, and sensing devices ranging from photonic crystals to drug-delivery carriers and nanoreactors.[2,3] Considering that tailoring the external morphology of hollow structures would endow them with unique properties, it is thus desirable to explore hierarchical hollow structures with various well-defined and novel geometrical architectures. Many recent efforts have been devoted to the controllable organization of primary building blocks into hierarchical hollow structures. To date, most reported hierarchical hollow structures are hollow spheres that are assembled from various nanobuilding units, such as nanowires,[4] nanorods,[5] nanobelts,[6] nanoribbons,[7] nanosheets,[8–12] nanocubes,[13,14] octahedron-like nanocrystals,[15] and hollow nanospheres.[16] In addition, hierarchical hollow cages, including rhombododecahedral silver cages,[17] cubic MoS_2 cages,[18] and octahedral and cubic $Cu_{2-x}Se$ cages,[19] have been obtained through different strategies. However, the synthesis of hierarchical hollow micro- and nanotubes has rarely been reported until now. Very recently, hierarchical tubular structures of CuS constructed from nanoflakes have been successfully synthesized by the groups of Yu and Xie.[20,21] Xu et al. reported the synthesis of a highly ordered array of hierarchical nanotubes constructed from Cu_2O hollow nanospheres by using a sacrificial template method.[22] In addition, in situ self-assembly of thin ZnO nanoplatelets into hierarchical mesocrystal microtubules

[a] B. Liu, Dr. Y. Xing, X. Liu, X. Sun, S. Hou, Prof. Z. Su
Department of Chemistry
Northeast Normal University
Changchun 130024 (China)
Fax: (+86) 431-85099108
E-mail: xingyan69cn@yahoo.com.cn
zmsu@nenu.edu.cn

[b] S. Wei
College of Chemistry
Jilin University
Changchun 130012 (China)

[c] Dr. D. Liu, Prof. Z. Shi
State Key Laboratory of Inorganic Synthesis and Preparative Chemistry of Jilin University
Changchun 130012 (China)

Supporting information for this article is available on the WWW under http://dx.doi.org/10.1002/chem.200903384.

with surface grafting of nanorods has been demonstrated.[23] Pan et al. prepared worm-like silica nanotubes by a simple sol-gel method.[24]

As one of the most complicated metal chalcogenides (variations in phases and stoichiometric compositions), cobalt sulfides are of particular interest as a result of their unique catalytic, electrical, optical, and magnetic properties and their potential applications in hydrodesulfurization and hydrodearomatization in many industrial fields.[25–27] In addition, cobalt sulfides have also been used in solar cells because of their high solar absorption, which is due to the strong intrinsic absorption coupled with surface morphology effects.[28] Due to these important properties, many recent efforts have been dedicated to the synthesis of micro- and nanocrystals of cobalt sulfides with various morphologies, such as Co_9S_8 and CoS_2 nanoparticles,[29] CoS nanowires,[30,31] thin films,[32] octahedrons of Co_3S_4,[25] and sea urchin-like Co_9S_8.[33] It is worth noting that Co_3S_4 nanotubes[34] and cobalt sulfide hollow nanocrystals[35] have been fabricated based on the Kirkendall effect. However, to the best of our knowledge there has been no report on the synthesis of hierarchical tubular structures of cobalt sulfide. Herein, we present a one-pot complex–surfactant-assisted hydrothermal method for growth of unusual $Co_{1-x}S$ ($x=0.75$) worm-like microtubes assembled by hexagonal nanoplates in high yield. The forming mechanism of the novel hierarchical-structured cobalt sulfides was proposed in terms of the experimental results. In addition, the electrochemical and magnetic properties of $Co_{1-x}S$ were systematically studied.

Results and Discussion

Characterization of $Co_{1-x}S$ hierarchical microtubes: The phase compositions and phase structures of the samples were examined by X-ray powder diffraction (XRD). As shown in Figure 1, all the diffraction peaks can be indexed to pure hexagonal phase $Co_{1-x}S$ with lattice constants $a=0.3380$ nm and $c=0.5185$ nm (JCPDS card No. 42-0826). No other impurity peaks were detected. Further evidence for the chemical composition of the cobalt sulfide was investigated by XPS. Figure 2 shows the XPS spectra obtained from the Co and S regions of the $Co_{1-x}S$. The Co 2p spectrum (Figure 2a) has a peak at 778.4 eV that can be attributed to sulfided Co–S, whereas the emission peak at 781.0 eV could be from oxidized Co–O because cobalt ions have a very strong affinity for atmospheric oxygen. A broadened peak at higher binding energies can be attributed to a satellite signal. In the S 2p spectrum (Figure 2b), the peak at 162.1 eV corresponds to the binding energies of Co–S.[25] There is also a peak for O impurity, due to the surface absorption of the samples exposed to air during processing.

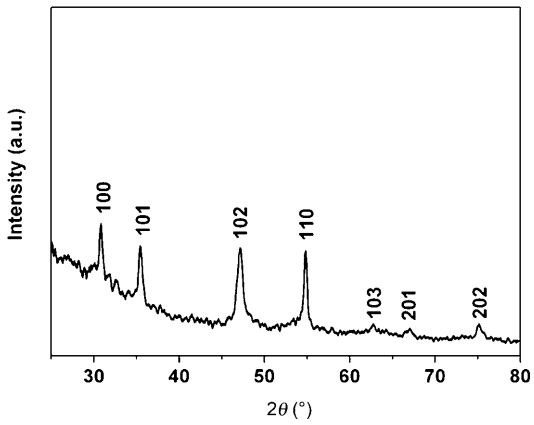

Figure 1. XRD pattern of $Co_{1-x}S$ microtubes obtained after 24 h at 160 °C.

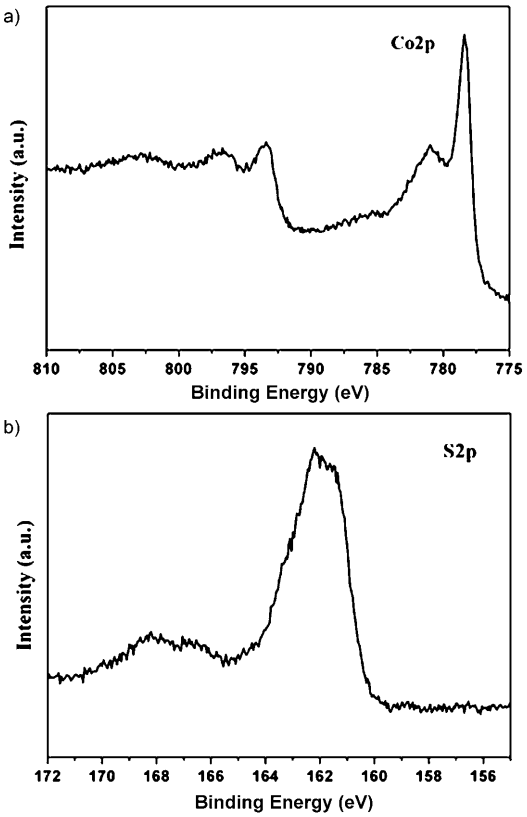

Figure 2. XPS spectra of a) Co 2p and b) S 2p for $Co_{1-x}S$ microtubes.

The morphologies of the products synthesized by hydrothermal treatment at 160 °C for 24 h were examined by field-emission scanning electron microscopy (FE-SEM). A large number of well-defined, worm-like, one-dimensional (1D) $Co_{1-x}S$ microstructures with an average length of about 15 μm were formed, as shown in Figure 3a. No other morphologies were detected, indicating a high yield of these worm-like microstructures. Figure 3b shows a high-magnification SEM image of the samples that reveals that the surface of the 1D microstructure is not smooth. More detailed morphologies (shown in Figure 3c and d) show that the surface of the worm-like 1D structure is assembled from numerous interleaving hexagonal nanoplates that have a side length of around 90 nm and a thickness of 22 nm.

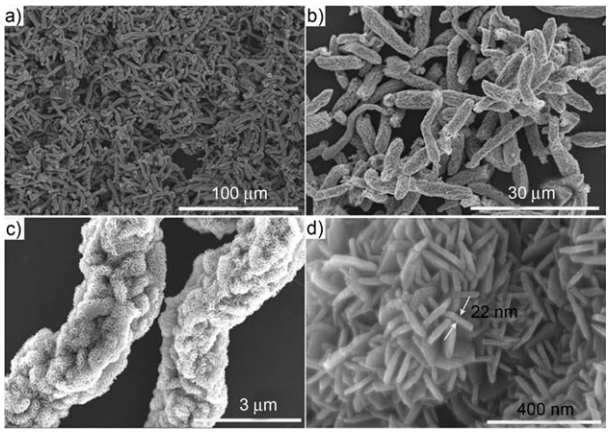

Figure 3. Low magnification (a,b) and high magnification (c,d) SEM images of the as-synthesized $Co_{1-x}S$ microtubes.

The morphology and interior structures of the 1D microstructures were further investigated by transmission electron microscopy (TEM). The TEM image of the as-prepared $Co_{1-x}S$ is shown in Figure 4a. The obvious contrast between

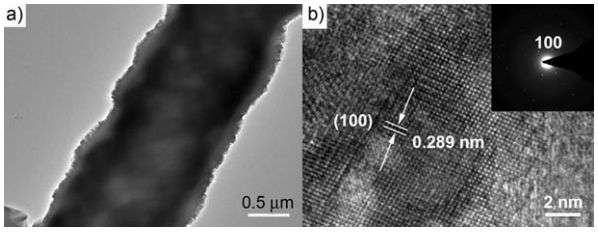

Figure 4. a) TEM image of the hollow $Co_{1-x}S$ nanotube and b) HRTEM image of the $Co_{1-x}S$ nanoflake (inset shows the SAED pattern).

the dark edge and pale center confirms the hollow structure of the 1D microstructure. The exterior diameter of the tube was about 1.5 μm, with a wall thickness about 400 nm. The above results demonstrate that large-scale $Co_{1-x}S$ worm-like microtubes with a hierarchical surface and hollow inner structure have been successfully fabricated. Because of its unique architecture, this novel hierarchical microtube might find applications in areas such as delivery systems, storage systems, catalysis, chemical sensing, and separation. The hierarchical structural wall creates a large specific surface area, which was measured by using the Brunauer–Emmett–Teller (BET) technique and found to be 46.24 $m^2 g^{-1}$(see Figure S1 in the Supporting Information). To confirm the chemical stoichiometry of the synthesized products, we performed energy-dispersive X-ray spectroscopy (EDX). A representative EDX pattern recorded for the microtubes revealed that the hierarchical structures are composed of Co, S, and C, and the ratio of cobalt to sulfur atoms is 0.75:1.

Further structural characterization of the $Co_{1-x}S$ microtubes was gained by using small-angle electron diffraction (SAED) and high-resolution TEM (HRTEM). The SAED pattern (Figure 4b, inset) shows that the nanoplates are single crystals with a hexagonal phase corresponding to $Co_{1-x}S$. Figure 4b shows a representative HRTEM image of a nanoplate. Lattice fringes with spacings of 0.289 nm are clearly visible, which agrees well with the lattice spacing of (100).

The possible growth mechanism of $Co_{1-x}S$ hierarchical microtubes: To reveal the morphology evolution of the hierarchical tubular structures of $Co_{1-x}S$, time-dependent shape evolution experiments were performed by intercepting intermediate products at different reaction stages under 160 °C. In the initial stage, an examination of the intermediate products collected after thermal treatment for 30 min shows the existence of a large number of irregular nanoplates (Figure 5a). After a reaction time of 1 h, some nanoplates began to interconnect randomly, as shown in Figure 5b. After 2 h, the dominant morphology of the product is worm-like mi-

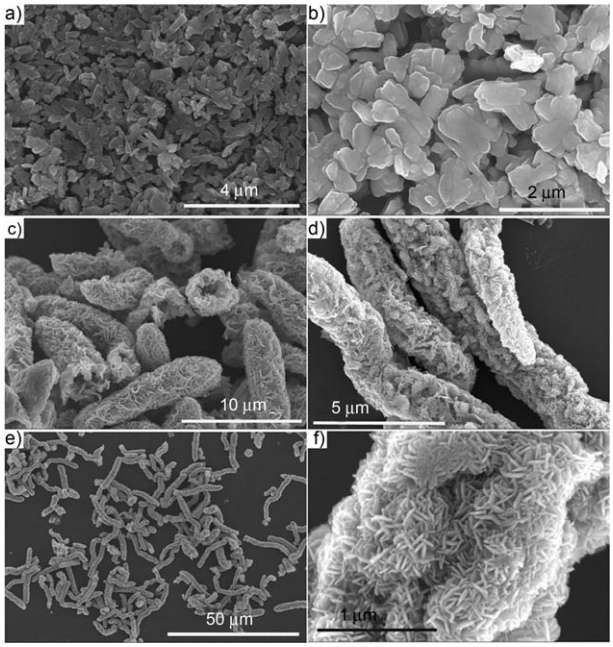

Figure 5. SEM images of samples obtained by hydrothermal treatment at 160 °C for different time intervals: a) 0.5, b) 1, c) 2, and d) 5 h. e,f) Low and high magnification SEM images, respectively, for the product after 10 h.

crostructures that are built from many interleaving but extensive curling nanoplates (Figure 5c), and the hollow interior structure can clearly be seen from the open ends of the worms. After a reaction time of 5 h, the curling nanoplates on the surface of some tubes gradually crystallize into hexagonal nanoplates, as shown in Figure 5d. As the reaction proceeded further, an ultrahigh yield of hierarchical tubular structures assembled from well-defined hexagonal nanoplates was obtained, as shown in Figure 5e and f.

To develop a comprehensive understanding of the formation mechanism of the hierarchical worm-like $Co_{1-x}S$ microtubes, we further investigated the influence of varying the

experimental parameters on the assembled morphology. It is known that organic surfactants can act as structure-directing agents or "soft templates" and are widely used to prepare nanostructured materials with peculiar morphologies. To investigate the influence of cetyltrimethylammonium bromide (CTAB) on the shape evolution in our current synthesis, a control experiment was carried out in the absence of CTAB, with the other parameters kept the same. It was found that no microtubes formed under these conditions, but aggregated flowerlike nanospheres together with a few nanoparticles were observed instead (see Figure S2a in the Supporting Information). Another experiment was carried out by using an appropriate dosage of poly(vinylpyrrolidone) (PVP; K30) as the soft template. However, only irregular nanoplates and nanospheres composed of nanoplates were obtained (see Figure S2b in the Supporting Information) under similar conditions. If poly(ethylene glycol)-block-poly(propylene glycol)-block-poly(ethylene glycol) (P123) was used instead of CTAB, the products were mainly nanorods with a rough surface (see Figure S2c in the Supporting Information). Experiment carried out by substituting CTAB with sodium dodecyl sulfate (SDS) gave a product of nanoparticles with a size of about 300 nm (see Figure S2d in the Supporting Information).

Ethylenediamine (en) is known to be a strong chelating agent that can form a complex with metal ions.[36] The influence of en on the $Co_{1-x}S$ microtubes was also investigated. For comparison, an experiment was carried out in the absence of en. A typical SEM image is presented in Figure S3 in the Supporting Information, and indicates that the product contains only irregular aggregates. The main reason for this observation is likely to be that the reaction rate of Co^{2+} and S^{2-} is too fast under these conditions. Here, the function of en is to form a complex with Co^{2+} ions through a coordination interaction that controls the release rate of Co^{2+} from the complex, thus lowering the precipitation rate of CoS and enhancing the product regularity. Based on the outcomes of the above experiments, we believe that both the CATB soft template and the en complexation play important roles in the formation of hierarchical $Co_{1-x}S$ microtubes.

The S source in our experiments also plays a vital role in the formation of the as-obtained hierarchical tubular structure. Parallel experiments were carried out by substituting thioacetamide (TAA) with L-cysteine, Na_2S, and CS_2, respectively. As shown in Figure S4 in the Supporting Information, only irregular nanocrystals can be formed under these conditions. Moreover, when the reaction temperature is decreased to 120 °C only irregular nanoparticles with an average size of 300 nm are observed (see Figure S5 in the Supporting Information). When the reaction temperature is increased to 200 °C, the products are still worm-like microtubes.

It is generally accepted that template-directed synthesis provides a simple and high-throughput procedure that also allows the complex topology present on the surface of a template to be duplicated in a single step.[37] The self-assembly of surfactant molecules in aqueous solution lead to the formation of micelles or vesicles that can act as soft templates for the synthesis of organic and inorganic hollow structures.[38] A previous report showed that in some surfactant systems, long worm-like micelles form at higher concentration.[39] The molecules of CTAB organize into worm-like micelles at the concentration used in our experiments, which may act as a "soft template" for preparing the worm-like microtubes of $Co_{1-x}S$. The formation mechanism of $Co_{1-x}S$ samples may involve the following steps: First, a Co^{2+} ion coordinates with an en molecule to form $[Co(en)_3]^{2+}$, while TAA is hydrolyzed to give S^{2-} in the base environment. Then Co^{2+} ions (slowly released from the Co^{2+}–en complex) react with S^{2-} to form 2D $Co_{1-x}S$ nanoplates, the formation of which is based on the traditional nuclei formation growth theory.[40] Driven by minimization, the chemical potential of the tiny nanoplates, and the total energy of the system, the small primary nanoplates can stack or connect to each other. Subsequently, hierarchical tubular microstructures can be formed by the aggregation and deposition of the nanoplates and by the oriented function of worm-like micelles of CTAB. As the growth continues, the curling nanoplates on the walls of the tubes are transformed into well-defined hexagonal nanoplates. On the basis of the above results, a schematic illustration of the possible formation mechanism of the $Co_{1-x}S$ worm-like microtubes is presented in Scheme 1.

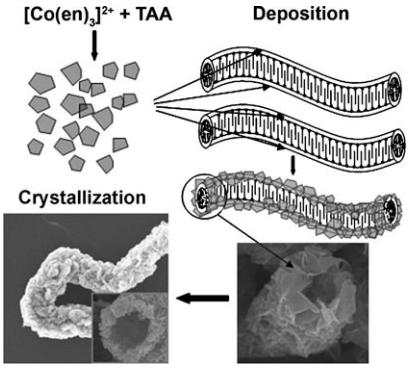

Scheme 1. Schematic illustration of the formation processes of hierarchical worm-like $Co_{1-x}S$ microtubes.

Electrochemical properties: Figure 6 shows the cyclic voltammetry (CV) curves of electrodes fabricated from $Co_{1-x}S$ with aqueous 6 M KOH as the electrolyte at various scan rates. The shapes of the CV curves show that the capacitive characteristic of the cobalt sulfide is distinguishable from that of the electric double-layer capacitance, for which the CV curve is close to the ideal rectangular shape. Two pairs of redox peaks can be observed in the CV curves and the peak currents are linearly proportional to the sweep rate, which suggests that the capacitance mainly results from the pseudocapacitive capacitance caused by two quasi-reversible electron-transfer processes. A previous report suggests that the redox transitions of cobalt sulfide in alkaline system

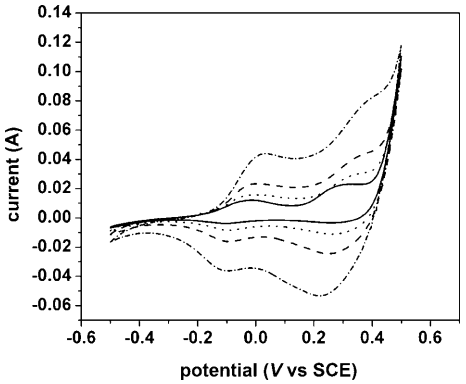

Figure 6. The CV curves of electrodes fabricated from cobalt sulfide (electrolyte: 6 M KOH) at various scan rates: 5 (——), 10 (•••••), 20 (– – –), and 50 mV s^{-1} (–•–•).

should take place between different valence states of cobalt.[26] The electrochemical redox reaction can be assumed to be as follows:

$$CoS+OH^- \underset{\text{discharge}}{\overset{\text{charge}}{\rightleftharpoons}} CoSOH+H_2O+e^- \quad (1)$$

$$CoSOH+OH^- \underset{\text{discharge}}{\overset{\text{charge}}{\rightleftharpoons}} CoSO+H_2O+e^- \quad (2)$$

Figure 7 shows the charge–discharge behavior of the $Co_{1-x}S$ electrode between −0.3 and 0.35 V at a current density of 5 mA cm^{-2}; the shape of the discharge curve does not show the capacitance characteristics of a pure double-layer capacitor, which is in agreement with the results of the CV

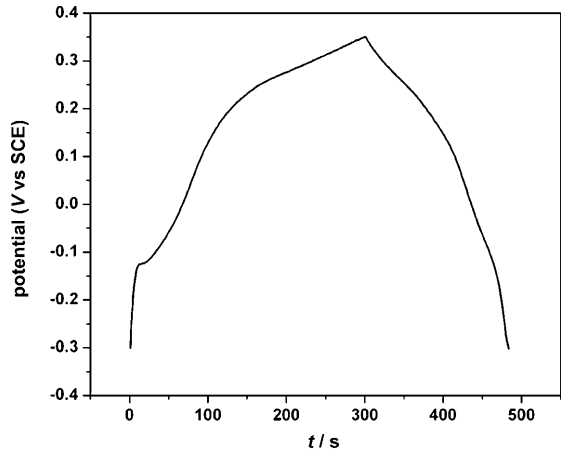

Figure 7. Charging–discharging behavior of a cobalt sulfide electrode at a current density of 5 mA cm^{-2} in 6 M KOH electrolyte.

curves. A nonlinear variation in potential versus time (−0.1 ~ 0.35) indicates typical pseudocapacitance behavior caused by the electrochemical redox reaction at the interface between electrode and electrolyte, whereas a variation in potential versus time (−0.3 ~ −0.1) parallel to the potential axis indicates pure double-layer capacitance behavior from the charge separation at the electrode–electrolyte interface. The specific capacitance (C) of the cobalt sulfide compound in the electrode is calculated from the discharge curve by $C=I\Delta t/(m\Delta V)$, in which I is the discharge current, m is the mass of the compound, ΔV is the potential window during discharge and Δt is the total discharge time. The specific capacitance value is 201 F g^{-1}, which is quite low compared with a previously reported cobalt sulfide nanowire (508 F g^{-1}).[30] This may be due to the more slack structure and larger specific surface area of the cobalt sulfide nanowires.

Magnetic properties: The magnetic characterization of the samples was performed by using a superconducting quantum interference device (SQUID) magnetometer. Magnetic properties of the $Co_{1-x}S$ microtubes are derived from zero-field-cooled and field-cooled (ZFC and FC) curves and from magnetization curves at 5 K. The results of ZFC and FC temperature-dependent measurements performed on $Co_{1-x}S$ microtubes with a 0.01 T field are shown in Figure 8. The FC curve shows a uniform decay and reaches the ZFC curve close to the peak, which indicates the superparamagnetic behavior at high temperature. For ZFC measurement, the sample was cooled from room temperature to 2 K without applying an external magnetic field. For the FC experiment, the sample was cooled from room temperature under an applied magnetic field of 5.0 T. Subsequently, the sample magnetization was recorded under an external magnetic field of 0.01 T as the temperature was increased. The ZFC curve exhibits a broad peak at the blocking temperature, T_B, of 7.8 K (Figure 8, inset), which corresponds to the Néel transition. At low temperatures, the FC magnetization rapidly increases with decreasing temperature, becoming about four times larger than the ZFC magnetization at $T=2$ K. This low-temperature behavior of the FC magnetization curve can be attributed to the surface spins, which are

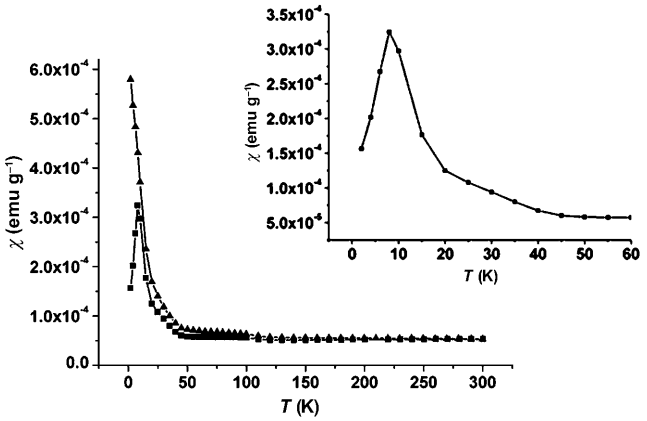

Figure 8. ZFC (■) and FC (▲) magnetization curves of $Co_{1-x}S$ measured under an applied magnetic field, H, of 0.01 T as a function of temperature. The cooling field was 5.0 T. Inset: An extended part of the ZFC curve, $T_B=7.8$ K.

frozen in the external field direction. At higher temperatures, the particle moments are free to undergo thermal fluctuations and the ZFC and FC curves merge together.

Below T_B, at 5 K, we measured the hysteresis loop (M–H curve) of $Co_{1-x}S$ microtubes. Figure 9 shows the small hysteresis loop at lower field at 5 K, which indicates the existence of a weak ferromagnetic component. This result suggests that the obtained $Co_{1-x}S$ microtubes are ferromagnetic at low temperature. The magnetic hysteresis loops show the coercive force (H_c) value and the saturated magnetic (M_s) moment at 5.0 K are 300 Oe and 1.008 emu g^{-1}, respectively. These results suggest that there are strong interactions between the nanoparticles of $Co_{1-x}S$ microtubes that result in a high M_s value.

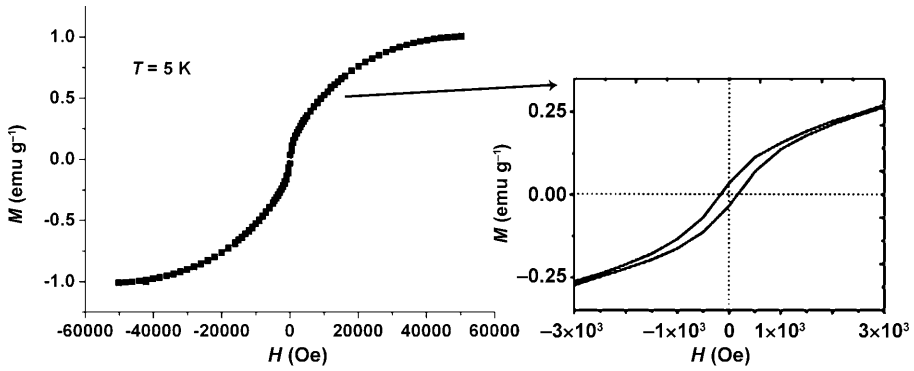

Figure 9. Magnetization (M) versus magnetic field (H) of $Co_{1-x}S$ was recorded at 5.0 K from −50000 to 50000 Oe. Inset: The enlarged magnetization curve between −3000 and 3000 Oe.

Conclusion

We have demonstrated a facile one-pot hydrothermal synthesis of unusual hierarchical worm-like $Co_{1-x}S$ microtubes assembled from hexagonal nanoplates with the assistance of CTAB and en. Experiments indicated that the surfactant, complexing agent, S source, and reaction temperature could affect the formation and morphology of the product. The possible formation mechanism of the novel hierarchical-structured cobalt sulfides was presented in detail. Electrochemical measurements indicated that the specific capacitance of $Co_{1-x}S$ microtubes is 201 F g^{-1}. The magnetic characterization suggests that the obtained $Co_{1-x}S$ microtubes are ferromagnetic at low temperature. These unusual hierarchical tubular microstructures have potential applications in areas such as delivery systems, storage systems, electronics, and catalysis. This simple and efficient approach demonstrates new capacities of template-assisted synthesis in the architecture of hollow structures and in construction of structurally complex nanomaterials.

Experimental Section

Chemicals: Cobaltous acetate tetrahydrate ($Co(CH_3COO)_2{\cdot}4H_2O$), thioacetamide (TAA), ethylenediamine (en), sodium sulfide (Na_2S), carbon disulfide (CS_2), L-cysteine, cetyltrimethylammonium bromide (CTAB), poly(vinylpyrrolidone) (PVP), and sodium dodecyl sulfate (SDS) were purchased from the Beijing Chemical Reagent Company. Poly(ethylene glycol)-block-poly(propylene glycol)-block-poly(ethylene glycol) (P123) was purchased from Sigma-Aldrich.

Synthesis: All chemical reagents were of analytical grade and were used without further purification. Typically, ethylenediamine (en; 4 mL) was added to a solution of $Co(CH_3COO)_2$ (0.1 mmol) in deionized water (4 mL) with stirring. After the solution turned yellow, CTAB (0.05 g) and TAA (0.3 mmol) were added sequentially. After stirring for 15 min, the resulting mixture was transferred into a Teflon-lined stainless steel autoclave and heated at 160 °C for 24 h. After the autoclave was allowed to cool to RT, the black products were separated by centrifugation, washed several times with distilled water and ethanol, and then dried under vacuum at 60 °C for 4 h.

Characterization: X-ray powder diffraction (XRD) analysis was measured by using a Siemens D5005 diffractometer with $Cu_{K\alpha}$ radiation (λ = 1.5418 Å). Field-emission scanning electron microscopy (FE-SEM) images were obtained by using a XL30 ESEM FEG microscope. Transmission electron microscopy (TEM) and high-resolution transmission electron microscopy (HRTEM) images were obtained by using a JEM-2100F microscope with an accelerating voltage of 200 kV. A Thermo ESCALAB 250 X-ray photoelectron spectrometer equipped with a standard and monochromatic source ($Al_{K\alpha}$; $h\nu$ = 1486.6 eV) was employed for surface analysis. The Brunauer–Emmett–Teller (BET) surface area was measured by using a Micromeritics Tristar 3000 analyzer at 77.4 K. The magnetic properties of the samples were measured by using Quantum Design SQUID MPMS XL-7 instruments. All electrochemical measurements were conducted by using a PARSTAT 2273 electrochemical workstation (USA). The working electrodes of the ECs were fabricated by mixing the prepared powder with acetylene black (25 wt %) and poly(tetrafluorene ethylene) (PTFE) binder (5 wt %). A small amount of distilled water was added to the mixture to produce a more homogeneous paste. The mixture was pressed on to nickel foam current-collectors to make electrodes. Electrochemical characterization was carried out in a conventional three-electrode cell with 6 M KOH as the electrolyte. Platinum foil and a saturated calomel electrode (SCE) were used as the counter and reference electrodes, respectively.

Acknowledgements

This work was supported by Jilin Province (20090518), the Department of Science and Technology of Jilin Province (20082103), the Training Fund of NENU'S Scientific Innovation Project (NENU-STC07004), and the Opening Fund of State Key Laboratory of Inorganic Synthesis and Preparative Chemistry of Jilin University.

[1] L. J. Lauhon, M. S. Gudiksen, D. L. Wang, C. M. Lieber, *Nature* **2002**, *420*, 57–61.
[2] Y. Zhao, L. Jiang, *Adv. Mater.* **2009**, *21*, 3621–3638.

[3] A. D. Dinsmore, M. F. Hsu, M. G. Nikolaides, M. Marquez, A. R. Bausch, D. A. Weitz, *Science* **2002**, *298*, 1006–1009.
[4] L. F. Xiao, Y. Q. Zhao, J. Yin, L. Z. Zhang, *Chem. Eur. J.* **2009**, *15*, 9442–9450.
[5] B. Liu, H. C. Zeng, *Chem. Mater.* **2007**, *19*, 5824–5826.
[6] B. J. Xi, S. L. Xiong, D. C. Xu, J. F. Li, H. Y. Zhou, J. Pan, J. Y. Li, Y. T. Qian, *Chem. Eur. J.* **2008**, *14*, 9786–9791.
[7] B. Liu, H. C. Zeng, *J. Am. Chem. Soc.* **2004**, *126*, 8124–8125.
[8] P. T. Zhao, T. Huang, K. X. Huang, *J. Phys. Chem. C* **2007**, *111*, 12890–12897.
[9] Y. Wang, Q. S. Zhu, H. G. Zhang, *Chem. Commun.* **2005**, 5231–5233.
[10] D. Chen, J. H. Ye, *Adv. Funct. Mater.* **2008**, *18*, 1922–1928.
[11] M. W. Xu, L. B. Kong, W. J. Zhou, H. L. Li, *J. Phys. Chem. C* **2007**, *111*, 19141–19147.
[12] J. K. Yuan, K. Laubernds, Q. H. Zhang, S. L. Suib, *J. Am. Chem. Soc.* **2003**, *125*, 4966–4967.
[13] L. Y. Chen, Y. G. Zhang, W. Z. Wang, Z. D. Zhang, *Eur. J. Inorg. Chem.* **2008**, 1445–1451.
[14] S. H. Yu, H. Cölfen, M. Antonietti, *J. Phys. Chem. B* **2003**, *107*, 7396–7405.
[15] X. Wang, F. L. Yuan, P. Hu, L. J. Yu, L. Y. Bai, *J. Phys. Chem. C* **2008**, *112*, 8773–8778.
[16] M. H. Yu, H. N. Wang, X. F. Zhou, P. Yuan, C. Z. Yu, *J. Am. Chem. Soc.* **2007**, *129*, 14576–14577.
[17] J. H. Yang, L. M. Qi, C. H. Lu, J. M. Ma, H. M. Cheng, *Angew. Chem.* **2005**, *117*, 604–609; *Angew. Chem. Int. Ed.* **2005**, *44*, 598–603.
[18] L. N. Ye, W. Guo, Y. Yang, Y. F. Du, Y. Xie, *Chem. Mater.* **2007**, *19*, 6331–6337.
[19] H. L. Cao, X. F. Qian, J. T. Zai, J. Yin, Z. K. Zhu, *Chem. Commun.* **2006**, 4548–4550.
[20] J. Y. Gong, S. H. Yu, H. S. Qian, L. B. Luo, X. M. Liu, *Chem. Mater.* **2006**, *18*, 2012–2015.
[21] Z. Y. Yao, X. Zhu, C. Z. Wu, X. J. Zhang, Y. Xie, *Cryst. Growth Des.* **2007**, *7*, 1256–1261.
[22] J. Xu, Y. B. Tang, W. X. Zhang, C. S. Lee, Z. H. Yang, S. T. Lee, *Cryst. Growth Des.* **2009**, *9*, 4524–4528.
[23] M. S. Mo, S. H. Lim, Y. W. Mai, R. K. Zheng, S. P. Ringer, *Adv. Mater.* **2008**, *20*, 339–342.
[24] L. P. Yang, P. Zou, C. Y. Pan, *J. Mater. Chem.* **2009**, *19*, 1843–1849.
[25] S. J. Bao, Y. B. Li, C. M. Li, Q. L. Bao, Q. Lu, J. Guo, *Cryst. Growth Des.* **2008**, *8*, 3745–3749.
[26] F. Tao, Y. Q. Zhao, G. Q. Zhang, H. L. Li, *Electrochem. Commun.* **2007**, *9*, 1282–1287.
[27] J. Wang, S. H. Ng, G. X. Wang, J. Chen, L. Zhao, Y. Chen, H. K. Liu, *J. Power Sources* **2006**, *159*, 287–290.
[28] G. B. Smith, A. Ignatiev, G. Zajac, *J. Appl. Phys.* **1980**, *51*, 4186.
[29] X. F. Qian, X. M. Zhang, C. Wang, Y. Xie, Y. T. Qian, *Inorg. Chem.* **1999**, *38*, 2621–2623.
[30] S. J. Bao, C. M. Li, C. X. Guo, Y. Qiao, *J. Power Sources* **2008**, *180*, 676–681.
[31] J. P. Ge, Y. D. Li, *Chem. Commun.* **2003**, 2498–2499.
[32] F. Srouji, M. Afzaal, J. Waters, P. O'Brien, *Chem. Vap. Deposition* **2005**, *11*, 91–94.
[33] X. H. Liu, *Mater. Sci. Eng. B* **2005**, *119*, 19–24.
[34] X. Y. Chen, Z. J. Zhang, Z. G. Qiu, C. W. Shi, X. L. Li, *J. Colloid Interface Sci.* **2007**, *308*, 271–275.
[35] Y. D. Yin, C. K. Erdonmez, A. Cabot, S. Hughes, A. P. Alivisatos, *Adv. Funct. Mater.* **2006**, *16*, 1389–1399.
[36] M. Wen, Y. F. Wang, F. Zhang, Q. S. Wu, *J. Phys. Chem. C* **2009**, *113*, 5960–5966.
[37] Y. N. Xia, P. D. Yang, Y. G. Sun, Y. Y. Wu, B. Mayers, B. Gates, Y. D. Yin, F. Kim, H. Q. Yan, *Adv. Mater.* **2003**, *15*, 353–389.
[38] H. L. Xu, W. Z. Wang, *Angew. Chem.* **2007**, *119*, 1511–1514; *Angew. Chem. Int. Ed.* **2007**, *46*, 1489–1492.
[39] Z. Lin, J. J. Cai, L. E. Scriven, H. T. Davis, *J. Phys. Chem.* **1994**, *98*, 5984–5993.
[40] Y. W. Jun, J. S. Choi, J. Cheon, *Angew. Chem.* **2006**, *118*, 3492–3517; *Angew. Chem. Int. Ed.* **2006**, *45*, 3414–3439.

Received: December 10, 2009
Published online: April 12, 2010

